Hydrogen-surfactant-assisted coherent growth of GaN on ZnO substrate

Jingzhao Zhang, Yiou Zhang, Kinfai Tse, and Junyi Zhu*
Department of Physics, the Chinese University of Hong Kong, Shatin, New Territories, Hong Kong, China

(Received 31 July 2017; revised manuscript received 29 November 2017; published 31 January 2018)

Heterostructures of wurtzite based devices have attracted great research interest because of the tremendous success of GaN in light emitting diodes (LED) industry. High-quality GaN thin films on inexpensive and lattice matched ZnO substrates are both commercially and technologically desirable. Intrinsic wetting conditions, however, forbid such heterostructures as the energy of ZnO polar surfaces is much lower than that of GaN polar surfaces, resulting in 3D growth mode and poor crystal quality. Based on first-principles calculations, we propose the use of surfactant hydrogen to dramatically alter the growth mode of the heterostructures. Stable H-involved surface configurations and interfaces are investigated with the help of our newly developed modelling techniques. The temperature and chemical potential dependence of our proposed strategy, which is critical in experiments, is predicted by applying the experimental Gibbs free energy of H_2. Our thermodynamic wetting condition analysis is a crucial step for the growth of GaN on ZnO, and we find that introducing H will not degrade the stability of ZnO substrate. This approach will allow the growth of high-quality GaN thin films on ZnO substrates. We believe that our new strategy may reduce the manufactory cost, improve the crystal quality, and improve the efficiency of GaN-based devices.

DOI: 10.1103/PhysRevMaterials.2.013403

I. INTRODUCTION

Semiconductors with wurtzite (WZ) structures have broad applications in modern semiconductor industry [1–6]. ZnO and GaN are two representative compounds. Practical device application with ZnO is not feasible due to inherent problems, e.g., the major difficulty in the *p*-type doping. Meanwhile, the lack of low cost and lattice matched substrates remains a great challenge for many group-III nitrides [7–9].

Devices based on ZnO/GaN heterostructures [3,10–12] have drawn research interests because of their similarities in the crystal structures, growth directions, and lattice constants. The lattice mismatch ratio is less than 2% [13,14] with ZnO being slightly larger. In recent years, ZnO wafers made from high-quality and large single crystalline using the hydrothermal growth method have been reported [15–17]. This method is currently thought to be at the threshold of mass production of ZnO crystals [18,19], indicating feasibility for commercialization [20]. Additionally, use of ZnO substrate may decrease the usage of expensive gallium for buffer layers. Therefore ZnO has been proposed to be an ideal substrate [21] or buffer layer [22] for GaN growth.

There are several experimental attempts to grow high-crystal-quality GaN on ZnO substrates [12,23–29]. Experimentally, it is difficult to form layer by layer type coherent growth, especially for molecular beam epitaxy (MBE) and organometallic vapor phase epitaxy (OMVPE) techniques at high temperature. Instead, 3D-like growth has been observed [12,28], with some interfacial layers of secondary phases like Ga_2O_3, Ga_2ZnO_4, and Zn_3N_2 [12,30–32]. Moreover, it has been shown that 3D-like growth persists even if the secondary phase layers are avoided [12]. On contrary, it is generally easier to grow ZnO on GaN substrates [30,31,33–35]. On top of a single-crystal GaN substrate, ZnO crystal films of high quality and sharp interfaces have been observed [31,34].

Theoretical analysis of these experimental observations is essential yet lacking. It shows that the surface energies of GaN polar surfaces are generally much higher than that of ZnO [36] with differences at the order of several tens of meV/Å^2, in agreement to the observed wetting difficulties of GaN on ZnO. Our previous theoretical works focused on the unreconstructed surface energy calculations and studies of the interfaces have not been included [36].

Surfactants can effectively modify the unfavorable growth mode [37,38]. In the past, surfactant studies have been mostly focused on large metallic elements [37–43], as large, nonvolatile, metallic elements are likely to float on top of the growth front. For example, arsenic as a surfactant was introduced in Si/Ge/Si(001) heterostructures to change growth modes in the late 1980s [37,38]. Whether small elements like hydrogen can serve as surfactants is an interesting and open question in the growth of GaN or ZnO [39,40,44–46]. There is some literature on H as a surfactant in a few other semiconductors. H as a surfactant may enhance the interchange mechanism in Si/Ge heterostructures [47]. H and Sb as dual surfactants were reported to enhance Zn incorporation in GaP [39].

During the standard OMVPE growth processes, hydrogen is a common impurity [48,49], often decomposed from precursors or carrier gases [50]. As a result, hydrogen-involved surface reconstructions have also been reported on the polar surfaces of ZnO [51–56] and GaN [57,58] both in experiments and theories. Such surface reconstructions are usually stable because H may passivate the surfaces to satisfy the electron-counting-rule (ECR) [59]. However, H atoms adsorbed on the

*jyzhu@phy.cuhk.edu.hk

surface may further diffuse into the bulk or desorb. To observe the H surfactant effect during epitaxial growth, fine control over the hydrogen partial pressure is crucial to maintaining proper surface coverage of hydrogen.

Despite these experimental challenges, hydrogen has advantages over large metallic surfactants: (1) H passivation to satisfy ECR is less specific in surface orientation, which allows this approach to be applicable to different surfaces of various materials; (2) H atom diffusion into bulk or interface can passivate dangling bonds and improve the crystal quality by suppressing the formations of certain deep defects [49,60,61]; and (3) H can be easily driven out by post-annealing treatment [62].

In order to guide experimental realization of the required growth conditions, it is essential to perform a calculation of the vibrational entropy of H, which is the most significant component of H chemical potential during high-temperature growth [52–55,57,63–67]. Applying experimental Gibbs free energy of H_2 is a possible alternative to quantitatively describe the relation between H chemical potential, temperature (T), and pressure (p), however, such practice is rare in theoretical analyses except a few works [40]. In addition to the temperature dependence of H chemical potential, hydrogen passivation on different surfaces of ZnO and GaN involves different numbers of H atoms, which complicates the analysis. Therefore the wetting conditions can be very sensitive to the H concentration on the surfaces. In this paper, we predicted the range of H chemical potential under typical growth temperature and pressure, within which desired layer by layer growth can be achieved. In addition to the thermodynamic analysis, a kinetic study on the surface or in the bulk can be also very important [68], yet, is out of the scope of this paper.

Due to the sensitive nature of H chemical potential dependence on the growth mode, an accurate estimation of absolute surface energies of the substrate materials, that of the epilayers, and the absolute interface energies is needed [37]. In this paper, we followed our previously developed methods for estimating absolute surface energies, and devised new strategies to calculate absolute interface energies [69,70]. Detailed discussions are included in methodology section. We believe our work is the first comprehensive thermodynamic analysis applied to a heterostructure along polar surfaces. Meanwhile, we calculated the phase diagram of a sharp ZnO/GaN interface. The wetting condition as a function of H chemical potential is obtained. Finally, based on all the above analyses, we obtained accurate predictions of proper growth conditions so that coherent growth of GaN thin films on ZnO substrates can be expected.

II. METHODOLOGY

Both kinetics and thermodynamics determine the crystal growth modes, in this paper, we focus our discussion on the thermodynamics point of view. The growth mode is determined by the free energy of the substrate surface (σ_s), the interface free energy (σ_i), and the surface free energy of the heteroepitaxial layer (σ_f). The inequality

$$\sigma_s > \sigma_i + \sigma_f \tag{1}$$

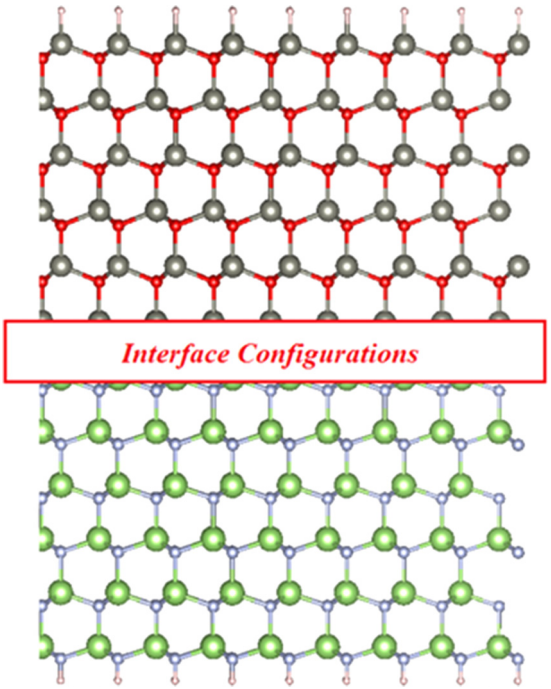

FIG. 1. A schematic illustration to the strategy of interface energy calculations, the bottoms on both sides are fully passivated with pseudo-H.

sets the condition for epitaxial films to wet substrates [37]. Proper wetting conditions can be determined only if all these three energies can be calculated accurately.

To estimate the absolute surface energies of GaN and ZnO, we adopted our recent approach that yields relatively accurate absolute surface energies of zinc-blende (111)/($\bar{1}\bar{1}\bar{1}$) and WZ (0001)/(000$\bar{1}$) surfaces [36,71]. The estimated errors are in the order of a few meV/Å^2 [36]. Early calculations were performed mainly on nonreconstructed surfaces. The accurate prediction of growth mode requires absolute energy accounting for surface reconstructions. In this paper, surface energies are evaluated using our cluster and pseudomolecule method [36], with structures adopted from surface reconstructions proposed by early STM observations and first-principles calculations [53,58,72,73].

The remaining challenge is to calculate an accurate interface energy. Here we constructed a simple slab model to calculate the interface energies of various interfacial configurations, especially for WZ materials. The structure is shown in Fig. 1. Both of the top and bottom surfaces are passivated with fractional-charged pseudo-H [74]. Since we can obtain the pseudochemical potentials (PCPs) of pseudohydrogen accurately, which are defined in our previous works [36,71], it is straightforward to further obtain the absolute interface energy by deducting the energy contributions from both surfaces. For any arbitrary interfacial configurations, absolute interface energies can be determined by the following equation:

$$\sigma_i = \frac{1}{\alpha_{\text{interface}}}\left(E_{\text{interface}} - \sum_i n_i \cdot \mu_i - n_{\text{H}_\text{A}}\hat{\mu}_{\text{H}_\text{A}} - n_{\text{H}_\text{B}}\hat{\mu}_{\text{H}_\text{B}}\right), \tag{2}$$

where $\alpha_{\text{interface}}$ is the area of the interface, $E_{\text{interface}}$ is the total energy of the fully passivated slab, shown in Fig. 1, n_i and μ_i are the numbers and chemical potentials of the slab atoms (e.g. Zn, O, Ga, N), n_{H_A} and n_{H_B} are the number of pseudo-H atoms used to passivate the bottom and top surfaces of the slab, and $\hat{\mu}_{H_A}$ and $\hat{\mu}_{H_B}$ are the PCPs of pseudo-H. Other interfaces with different polarities and configurations can be constructed similarly. It should be noted that the obtained absolute interface energies are directly comparable. This universal approach is superior to former modeling techniques on the interface energy calculations that utilized superlattice-like models containing at least two coupled interfaces [32,75,76], which suffered from problems induced by charge transfers and strong dipole-dipole interactions between the interfaces, inducing large artificial errors. In addition, our approach is able to isolate interfaces from each other, and the absolute interface energy of a single interface could be achieved even on asymmetric interfaces, while with traditional methods, only relative stabilities [32] or average interface energies [75] could be obtained in such cases.

Important surface reconstructions in previous works with and without H are calculated and discussed in this paper in relation to our calculated phase diagram shown later. The choices of low energy reconstructions without H follow previous investigations [53,58,72,73]. Specifically, on ZnO polar surfaces, although several different surface reconstruction models are proposed by both theoretical calculations and experiments [53,73], the surface energy differences among them are in the order of a few meV/Å^2 [73], suggesting that the (2×2) adatom reconstruction is adequate for our discussions here. For GaN, (2×2) adatom reconstructions were taken into consideration under the condition of N-rich enviroment [58], such reconstructions were suggested to be important under high-temperature growth [52].

For the reconstructions with H, while there are numerous possible H covered reconstructions, the lowest energy configurations are well represented by those surfaces that satisfy ECR [52,57]. It is demonstrated that the vibrational entropy of the surface plays a decisive role in the competition among various phases to achieve thermodynamic stability [53]. The temperature and pressure effects of the gas phase reservoirs, arising from vibrational contributions to the entropy [57], can be significant in high-temperature growth, and would favor reconstructions with less hydrogen atoms [57]. All configurations of reconstructions considered will be shown in latter sections. Although it is shown in Ref. [55] (see Fig. 13) that the surface reconstructions of (5×5) H4 and (5×5) H5 are also competing phases for the $-c$ plane of ZnO, we will show later that these phases would not affect our conclusion significantly.

A systematic comparison among all possible surface configurations and a detailed surface phase diagram are sometimes used to demonstrate the problems on surfaces [51,57,77,78]. However, this is not easily defined when it comes to a heterogeneous case, where more complex reconstructions than that in pure substance system may exist during the formation of heterostructures, especially for epitaxial films. Here we simplified the searching process and used the most energetic favorable configurations in ZnO or GaN to model the top surface of the heterostructures. We believed that our discussions on the selected detrimental reconstructions may still show the thermodynamic driving force to demonstrate the problem. In the unlikely case, even if we missed the lowest energy configuration in GaN, reconstructions with lower surface energies will not change our conclusion and are better for the realization of our strategies, as the inequality (1) showed.

The total energy calculations of bulks, slabs, and clusters [36] were based on density functional theory [79,80] as implemented in VASP code [81], with a plane-wave basis set [82,83] and PBE generalized gradient approximation (GGA) as the exchange-correlation functional [84]. GGA functional severely underestimates the band gap of GaN and ZnO, which may lead to wrong energy eigenvalues or electron occupations in the surface states [58]. Therefore we also performed calculations using the hybrid functional of Heyd, Scuseria, and Ernzerhof (HSE) [85,86] on slabs of polar surfaces and interfaces, as well as pseudomolecules [36]. Slabs for surface reconstructions were performed on 2×2 slabs containing ten bilayers, with a $9 \times 9 \times 1$ Gamma-centered k-point mesh for GGA and a $3 \times 3 \times 1$ mesh for HSE. For the H involved reconstructed (0001) surface of ZnO, 3×3 slabs and a $6 \times 6 \times 1$ k-point mesh were applied for GGA. In the case of interface energy calculations, we construct the ZnO/GaN interface with six bilayers ZnO and six bilayers GaN on 1×1 slabs for unreconstructed cases and 2×2 slabs for compensated cases. The k-point sampling is up to $15 \times 15 \times 1$ and $7 \times 7 \times 1$ for GGA, and $7 \times 7 \times 1$ and $3 \times 3 \times 1$ for HSE. The slabs were separated by a vacuum of at least 15 Å. All the atoms in the slab were allowed to relax until forces converged to less than 0.005 eV/Å for GGA calculations and 0.01 eV/Å for HSE calculations. The energy cutoff of the plane-wave basis set was set to 500 eV for GGA and 400 eV for HSE. We have done careful convergence tests for all of the settings aforementioned.

Calculations for the formation energies of related compounds are necessary for obtaining the thermodynamic phase diagram of interfaces shown later. There is a persistent difficulty to correctly estimate the formation energy of the possible secondary phase of Zn_3N_2 near the interfaces, which for both our calculations and previous works are positive due to the intrinsic problems of exchange correlation functional [87]. The calculated formation energies of compounds, such as II-VI or III-V, are always significantly different from the experimental ones [88], which are important to our further discussions. Therefore we applied and strictly followed the fitted elemental-phase reference energies (FERE) method [88–90] to achieve relatively accurate formation energies. In the FERE method, for GGA, totally 12 elements and 44 compounds were included; for HSE, totally 9 elements and 24 compounds were included. All the calculated data are summarized in Supplemental Material [91]. Readers can also refer to Refs. [88–90] for more calculation details.

III. RESULTS AND DISCUSSIONS

Firstly, secondary phases near interfaces may significantly increase interface energies and ruin the layer by layer growth mode. To obtain sharp interfaces, formations of any interlayers of possible secondary phases, including Zn_3N_2, Ga_2ZnO_4, and Zn_3N_2, must be suppressed. The calculated formation energies of the important compounds by FERE method in this study are listed in Table I. The calculated results are well consistent with the experimental values. Qualitatively, the FERE method

TABLE I. Calculated formation energies by the FERE method, with both GGA and HSE, compared with the experimental values.

	GGA (FERE)/eV	HSE (FERE)/eV	Exp./eV
ZnO	−3.53	−3.73	−3.62 [92]
GaN	−1.47	−1.41	−1.62 [93]
Zn_3N_2	−0.22	−0.26	−0.25 [92]
Ga_2O_3	−11.43	−11.74	−11.30 [92]

corrects the formation enthalpy of Zn_3N_2 from positive to negative. Such correction also slightly modified the phase diagram. The impact of FERE on the surface energy was also calculated and discussed, with details shown in Supplemental Material [91]. Still, this correction affects the prediction on the critical value of $\Delta\mu_H$, roughly with the order ∼0.1 eV, and thus should be included.

These results lead to the phase diagram of the Zn, O, Ga, N compounds, as shown in Fig. 2. The shadow part of the diagram is the chemical potential region in which only ZnO and GaN phases can form. Therefore nearly O-poor and N-rich growth condition is required to grow secondary-phase-free ZnO/GaN interfaces. This phase diagram is nearly functional-independent, with a growth window calculated by HSE being slightly larger than that of GGA. To make a clear demonstration, we focus our discussion on the comparison of results along the four sampling points (e.g., A, B, C, D for GGA and A′, B′, C′, D′ for HSE) in both phase diagrams simultaneously. Additionally, with the existence of H atoms, according to the calculated results, H_2O formation is excluded because such formation requires an O-richer chemical potential window than in ZnO growth is allowed. We also considered possible NO and NO_2 phases. Because their calculated formation enthalpies are positive or very close to zero (NO: GGA:1.29 eV, HSE:1.77 eV, and NO_2: GGA: −0.11 eV, HSE:0.54 eV), these two phases do not affect the phase diagram in both GGA and HSE cases. Nonetheless, when NH_3, whose formation enthalpy is −0.85 eV by GGA, −1.05 eV by HSE, and −0.48 eV by experiments [94], is included in the discussion, the phase diagram would indeed be affected. At low temperature, the H_2 entropy contribution could be neglected, resulting in a H-richer limit than at high temperature. The stable region could shrink along the negative direction of the vertical axis, namely, the rich limit of $\Delta\mu_N$, as the formation enthalpy of NH_3 must be suppressed by a proportionally poorer $\Delta\mu_N$, according to inequality (3). However, at high temperature, where the entropy of H_2 is significantly larger, and the value of $\Delta\mu_H$ would largely decrease, the inequality (3) can be satisfied even under the N-richest condition ($\Delta\mu_N$ equals to zero):

$$\Delta\mu_N + 3\Delta\mu_H \leqslant \Delta H_{NH_3}, \tag{3}$$

suggesting that the formation of NH_3 would be suppressed. This argument is consistent with the previous conclusion and the surface phase diagram shown in Ref. [57]. Under high-temperature condition, the whole stable chemical potential range shown in Fig. 2 would not be affected by the NH_3 phase. Due to the aforementioned reasons, the zero-temperature phase diagram shown in Fig. 2 should be a good approximation to a finite-temperature phase diagram, even at the high-temperature regime in which GaN growth is possible.

Another key issue for ZnO as a substrate is its stability under certain growth conditions. According to the phase diagram and the related discussions above, if H is incorporated into the system, no reactions between ZnO and GaN would occur, and the H would not degrade the stabilities of both ZnO substrates and GaN epilayers under high-temperature growth conditions. Previous experimental observations also confirm that the adsorption of H on the surfaces of GaN or ZnO is stable [53,55,57].

Next, we obtained the absolute surface energies of cleaved and reconstructed polar surfaces of ZnO and GaN. The surface energies of c and $-c$ planes were calculated, as shown in Fig. 3. Generally, the energies calculated by HSE are larger than that by GGA. The overall shapes along the sampling points of both sets of data, from GGA and HSE, are quite similar, indicating that there exist approximately constant shifts between the results based on the different functional. With reference to HSE functional, GGA largely underestimated the energies of cleaved surfaces. The errors of the GGA results are likely due to the fact that GGA functional underestimate the energies with empty orbitals. For ZnO, the surface energies of reconstructed c and $-c$ planes are close, with -c plane slightly higher than c plane. The energy difference obtained from HSE is slightly larger than that obtained from GGA. At A′, B′, and D′, namely O extremely poor points, the cleaved (0001) surface is slightly more stable than the (2×2) O adatom surface. In the GaN results, the surface energy of reconstructed c plane is slightly higher. We found that this is different from the

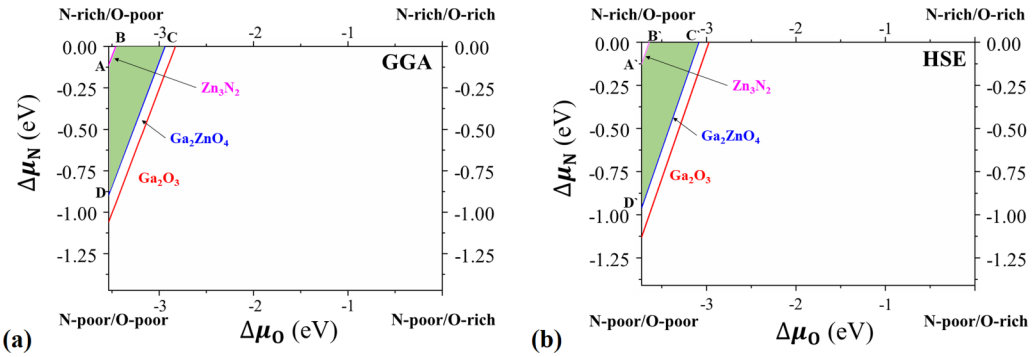

FIG. 2. Phase diagram of ZnO and GaN interfaces with GGA (a) and HSE (b) functional. The shadow part is the stable chemical potential region where no secondary phases can form. In both of the figures, four sampling points are selected, denoted by A, B, C, D and A′, B′, C′, D′.

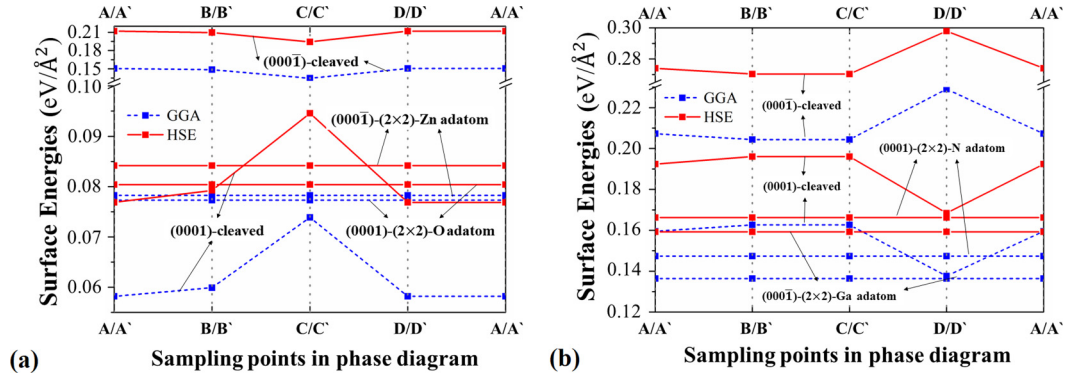

FIG. 3. Calculated absolute surface energies of cleaved and (2×2) reconstructed polar surfaces for ZnO (a) and GaN (b), along the sampling points in Fig. 2, with both GGA and HSE functionals.

results shown in Fig. 2 in Ref. [58]. This is possibly due to the inferior methodology adopted in Ref. [58] resulting in a stressed wedge structure and poor self-consistency of calculated surface energy [36,58], since the steric effect of H is significant. As discussed comprehensively in Ref. [36,71], our approach should give an improved accuracy with an error of about a few meV/Å^2.

Within the growth window shown in Fig. 2, configurations of sharp interfaces with no interlayers were considered; the absolute interface energies of these interfacial configurations are directly comparable. To quantify the error of lattice mismatch, the interfaces energies of ZnO/GaN heterostructures using the lattice constants of ZnO and that of GaN were both evaluated. The difference of interface energies between two choices of lattice constant is less than 3 meV/Å^2, such choices would not qualitatively affect our conclusions.

Next, we considered different interfacial configurations. Experimentally, it is observed that the epitaxial crystal has the same polarity as the substrate without interface modifications and substrate pretreatments [26,28,95]. Therefore all the interfacial configurations without adlayers are tested, furthermore, adlayer-inserted interfaces were also calculated. Out of totally 16 possible configurations, interfaces of [N-Ga-O-Zn] and [Ga-N-Zn-O] [96], which preserve the AB packing of WZ structure, are the most stable cases, as shown in Figs. 4(a) and 4(b). This indicates that when the epilayers have the same polarities as the substrates do, the interfaces are relatively stable. Both interfaces were also speculated by experimental groups [95]. However, unreconstructed interfaces may not be the most energetically favorable in all cases, since these interfaces can be negatively or positively charged. This suggests a possible strategy of reconstructing the interfaces, as suggested in Ref. [32], as shown in Figs. 4(c) and 4(d). The compensated interfacial configurations and energies are modeled and calculated from (2 × 2) cells, where introducing one cation substitution would fully satisfy ECR. Only the substitutions within one layer in the vicinity of the interfaces are considered. Even if there exist more stable interfacial configurations, the conclusion on the surfactant strategy would be unaffected as inequality (1) is still preserved.

The calculated absolute interface energies are shown in Fig. 5. For the cation-compensated interfaces, the absolute interface energies are low and almost functional-independent. While for the unreconstructed interfaces, HSE results appear to have a constant upward shift compared with the GGA results. In Fig. 5(a), at the points D/D′, GGA wrongly estimates the energy of unreconstructed interface [N-Ga-O-Zn] to be negative, lower than that of the cation-compensated one. While HSE shows that the unreconstructed interface energy is still higher than the compensated case. Therefore, in the following discussions, we only included the absolute interface energies of compensated cases. For the ease of experimentalists, who usually control the chemical potential of Ga, the plot of interface energies corresponding to the Ga chemical potential from Ga-poor conditions to Ga-rich, shown in Fig. 5(b), is also included. The chemical potential of Zn is set to be zero here, near the O-poor region in Fig. 2. The energies of cation-compensated interfaces are still independent of the chemical potential. As it changes from Ga-poor to Ga-rich, the unreconstructed interface [N-Ga-O-Zn] energy decreases and the unreconstructed interface [Ga-N-Zn-O] energy increases. At Ga-rich condition, the unreconstructed [N-Ga-O-Zn] would even be slightly more stable than the compensated one by the HSE functional due to the extra energy penalty of Ga.

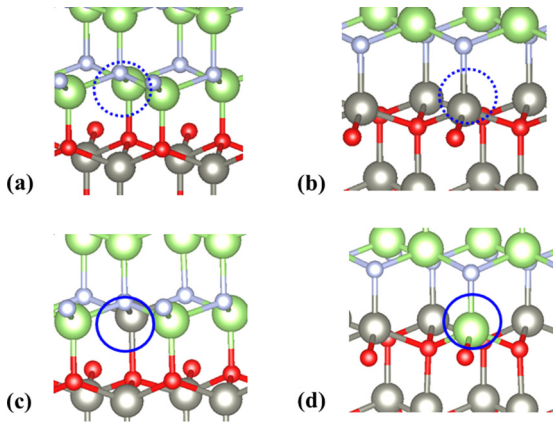

FIG. 4. Calculated interface configurations for ZnO/GaN heterostructures: (a) unreconstructed [N-Ga-O-Zn], (b) unreconstructed [Ga-N-Zn-O], (c) cation-compensated [N-Ga-O-Zn], and (d) cation-compensated [Ga-N-Zn-O]. (Green atoms for Ga, silver for N, grey for Zn, and red for O) The circled positions are the sites of the replacement.

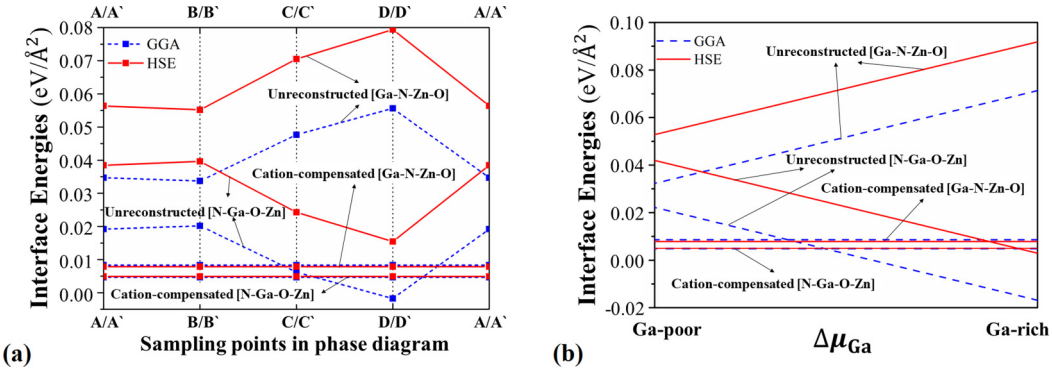

FIG. 5. Calculated absolute interface energies with the configurations shown in Fig. 4, (a) along the sampling points in Fig. 2, (b) with the relation of Ga chemical potential, by GGA and HSE functionals.

According to inequality (1) and the above calculation results, we obtained

$$\sigma_s[\mathrm{GaN}(0001)_{\mathrm{reconstructed}}] - \sigma_i[\mathrm{N-Ga-O-Zn}] - \sigma_f[\mathrm{ZnO}(0001)_{\mathrm{reconstructed}}] > 0, \quad (4)$$

$$\sigma_s[\mathrm{GaN}(000\bar{1})_{\mathrm{reconstructed}}] - \sigma_i[\mathrm{Ga-N-Zn-O}] - \sigma_f[\mathrm{ZnO}(000\bar{1})_{\mathrm{reconstructed}}] > 0, \quad (5)$$

these two inequalities suggest that the ZnO thin films wet both c and $-c$ directions of GaN substrates, but not vice versa. Furthermore, it may be very challenging to grow high-quality GaN thin films on ZnO substrates because of the large difference of more than 80 meV/Å^2 between the surface energies of ZnO and GaN along c or $-c$ directions. This is consistent with experimental observations [12,23–35]. This conclusion is independent of the functionals used.

The intrinsic wetting conditions do not align with the industrial needs of inexpensive and lattice-matched substrates for GaN. One of the possible strategies would be surfactant assisted growth. Proper choice of surfactant may tune the surface energies of ZnO and GaN to fulfill the wetting conditions, so that high-quality GaN can be grown on ZnO substrates achieving the layer by layer growth mode. In latter parts, we show that H may be one of such surfactants. Hydrogen may attach to the polar surfaces and form H-involved reconstructions of ZnO and GaN to lower the overall surface energies. According to the calculated growth window discussed above, growth of the heterostructures can only occur under N-rich, O-poor conditions. Therefore the configurations of H adsorbed surfaces with the lowest energies, as shown in Fig. 6, were adopted following early experimental and theoretical results. In this discussion, these reconstructions should also be compared with the adatom reconstructions. All of the configurations except (b) and (c) in Fig. 6 satisfy ECR.

For the c plane, the surface configurations shown in Fig. 6(a) for GaN and Figs. 6(b) and 6(c) for ZnO were considered and tested. The configurations in Figs. 6(b) and 6(c) represent two competing phases for the ZnO c plane [53]. All three configurations were evaluated by the GGA functional. At zero temperature, at point A of Fig. 2(a), the absolute surface energies are 77.6, 49.1, and 50.2 meV/Å^2, respectively; at point C, the absolute surface energies are 77.6, 43.5, and 37.5 meV/Å^2, respectively. With inclusion of the temperature effect, mainly H_2 entropy, the absolute surface energies of these surfaces dependent on the chemical potential of H, i.e., $\Delta\mu_H$. The energy difference between ZnO and GaN c plane increases with temperature, detailed analyses of this trend with figures are referred to Supplemental Material [91]. Along c direction, the absolute surface energy of GaN c plane remains larger than that of ZnO even with the inclusion of H, concluding that such surfactant strategy is ineffective on the c plane.

For the reconstructions of $-c$ planes, different numbers of H atoms may be involved on the most stable surface configurations. The following discussion is based on the premise that the surface energies of GaN can be lowered by H adsorptions, namely the configuration shown in Fig. 6(d). As for ZnO, to make a fair comparison, its surface configurations are also expected to be stable under the same stable chemical potential conditions (including H) of GaN surfaces. The free energy of the various ZnO surfaces is a function of H chemical potential. Both relevant cases, one with the $-c$ plane passivated by three H maintaining the same H concentration on the surface, the other with the same plane passivated by 2 H satisfying ECR as shown in Fig. 6(e), are included. Although in the case of three H, the absolute surface energies of GaN are much lower than that of ZnO, with a difference more than 27 meV/Å^2, the two-H case is the most stable configuration

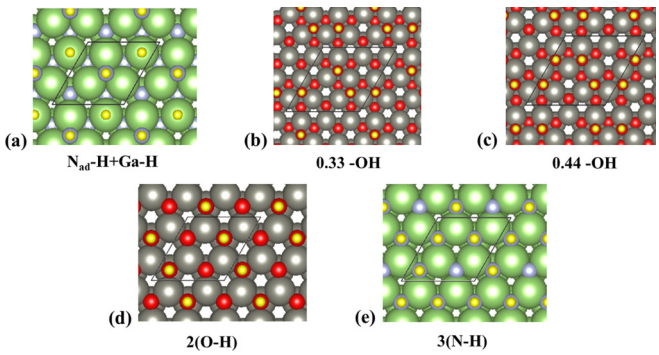

FIG. 6. Hydrogen involved (0001) and (000$\bar{1}$) surface reconstructions for GaN [(a) and (e)] and ZnO [(b), (c), and (d)]. The yellow atoms are H. Other atoms follow the notations in Fig. 4. The parallelogram in each configuration shows the smallest period of the surface structure.

with the same H chemical potential as that of the GaN surface. This result is also consistent with other previous theoretical calculations conducted on ZnO surfaces [55]. It is therefore most reasonable to compare the most stable configurations, i.e., Figs. 6(d) and 6(e), with the H chemical potential entering the absolute surface energy difference as a free parameter within the allowed thermodynamic limits.

We focus the remaining discussion on the $-c$ planes of ZnO and GaN, shown in Figs. 6(d) and 6(e), with both configurations fully satisfying ECR. The following relationship is desirable:

$$\sigma_s[\mathrm{ZnO}(000\bar{1})_{\mathrm{reconstructed}}] - \sigma_i[\mathrm{N-Ga-O-Zn}] - \sigma_f[\mathrm{GaN}(000\bar{1})_{\mathrm{reconstructed}}] > 0. \quad (6)$$

The surface energies of H-involved surfaces largely depend on H free energy μ_{H}, namely,

$$\sigma_{s-H} = \frac{1}{\alpha_{\mathrm{surface}}}\left(E_{\mathrm{slab}} - \sum_i n_i \cdot \mu_i - n_{\mathrm{H_X}}\hat{\mu}_{\mathrm{H_X}} - n_{\mathrm{H}}\mu_{\mathrm{H}}\right), \quad (7)$$

where E_{slab} is the total energy of the slab model, $\alpha_{\mathrm{surface}}$ is the surface area of the reconstructed surface, $n_{\mathrm{H_X}}$ is the number of corresponding pseudo-H atoms used to passivate the bottom, and $\hat{\mu}_{\mathrm{H_X}}$ is the PCPs of corresponding pseudo-H. More importantly, the comparison between the reconstructions with different number n_{H} of H can be conducted using the absolute surface energies computed by Eq. (7), given any chemical potential μ_{H} of H atoms. Here, μ_{H} can be expressed as

$$\mu_{\mathrm{H}} = \tfrac{1}{2}\left(E_{\mathrm{H_2}} + 2\Delta\mu_{\mathrm{H}}\right), \quad (8)$$

where $E_{\mathrm{H_2}}$ is the total energy of H_2 at zero temperature derived from DFT calculations, and $\Delta\mu_{\mathrm{H}}$ captures the chemical potentials relative to the total energy of the isolated molecule, determined by the gas atmospheric temperature and pressure. Quantitatively, this formula can be solved theoretically by the partition functions of diatomic ideal gases [57,63,97], which includes a sum over translational, rotational, and vibrational states [98]. As suggested by early literature, the vibrational state of H_2 is the main contribution under high growth temperature [57,63]. Besides this method, we noticed that another quantifiable relation of the quantity $\Delta\mu_{\mathrm{H}}$ is [98]

$$2N\Delta\mu_{\mathrm{H}} = G, \quad (9)$$

where N is the number of H_2 molecules, G is the Gibbs free energy of H_2 (gas) in reference to zero temperature. This quantity is referred to the experimental data of H_2 (gas) Gibbs free energy G [99], including both enthalpy and entropy contributions, to obtain the quantitative relation of the aforementioned expression.

The required $\Delta\mu_{\mathrm{H}}$, obtained by substituting Eqs. (7) and (8) into Eq. (6), where Eq. (6) can be critically satisfied, and the corresponding absolute surface energies of H-involved surfaces calculated according to Eq. (7) are shown in Table II. For the GaN H-involved reconstructed $(000\bar{1})$ surface, the surface energies are lower than the case of (2×2) adatom at the four sampling points in both GGA and HSE. While for ZnO, only at points C/C′ and D/D′, the H-involved reconstructed surface is more favorable than the case of (2×2) adatom. Generally, GGA and HSE give quite consistent predictions:

TABLE II. Hydrogen chemical potential relative to the total energy of the isolated molecule, denoted as $\Delta\mu_{\mathrm{H}}$, when the wetting condition is satisfied critically. It is shown along the sampling points illustrated in Fig. 2. The surface energies with the configurations shown in Figs. 6(d) and 6(e) at that stage are also calculated, denoted as $\sigma_{\mathrm{ZnO-H}}$ and $\sigma_{\mathrm{GaN-H}}$, and σ_{ZnO} represents the absolute surface energy of the (2×2) reconstructed surface of ZnO. Here, only the lowest surface energies of ZnO and GaN are shown in this table. The predicted maximum growth temperatures (under the pressure of 1 bar) for possible sampling points are denoted as T. The data with underlines are those that we should compare directly.

		A	B	C	D
GGA	$\Delta\mu_{\mathrm{H}}$/eV	−1.065	−1.099	−1.070	−0.782
	$\sigma_{\mathrm{ZnO-H}}$/meV/Å^2	–	–	**76.3**	**76.8**
	$\sigma_{\mathrm{GaN-H}}$/meV/Å^2	**73.6**	**73.6**	**71.3**	**71.9**
	σ_{ZnO}/meV/Å^2	**78.5**	**78.5**	–	–
	T/K ($p\sim1$ bar)	∼1400	∼1400	∼1400	∼1100
		A′	B′	C′	D′
HSE	$\Delta\mu_{\mathrm{H}}$ /eV	−1.106	−1.149	−0.995	−0.675
	$\sigma_{\mathrm{ZnO-H}}$/meV/Å^2	–	–	**71.4**	**71.4**
	$\sigma_{\mathrm{GaN-H}}$/meV/Å^2	**79.2**	**79.2**	**66.4**	**66.4**
	σ_{ZnO}/meV/Å^2	**84.2**	**84.2**	–	–
	T/K ($p\sim1$ bar)	∼1400	∼1400	∼1300	∼1000

at all of the four sampling points, the H-adsorbed GaN $-c$ surface has lower surface energies, this means that the growth temperature and partial pressures can be tuned towards the region near these sampling points, at which the hydrogen surfactant would overturn the intrinsic wetting conditions to satisfy inequality (6). Additionally, at A/A′ and B/B′, when $\Delta\mu_{\mathrm{H}}$ increased by ∼0.2 eV, reconstruction of (5×5) H4 and (5×5) H5 on the $-c$ plane of ZnO, as shown in Fig. 6(d) would take over the surface. These (5×5) phases dominate a quite small region in the whole surface phase diagram, however, such large period reconstructions could hardly exist in high-temperature epitaxial growth processes, which has been discussed in previous literature [57]. Moreover, similar to the discussions of reconstructions without H, large periodic structures like (6×6) ADC in Ref. [73] or n6 in Ref. [53] are also not considered in our discussion, because the energy differences between these configurations and the (2×2) adatom are within $3\sim4$ meV/Å^2, which means that the (2×2) adatom is a reasonable representative in our discussions. In the case of H involvement, the (2×2) configuration is also selected as a representative in the following discussions.

Since Eq. (9) relates $\Delta\boldsymbol{\mu}_{\mathbf{H}}$ and Gibbs free energies, the H chemical potential can be further expressed as a function of temperature and pressure by referring to the corresponding experimental Gibbs free energies data G of H_2 [99]. For a constant $\Delta\boldsymbol{\mu}_{\mathbf{H}}$, a lower pressure requires a lower temperature. We restrict the pressure to the value of 1 bar, which is typical for OMVPE growth. The typical H_2 pressure of MBE growth is of the order of 10^{-12} atm; the resulting critical temperature would be far lower than the typical value of 1000 K [67], and is thus neglected. For experimental realizations, the required H_2 pressure could be higher due to unavoidable passivation of

bulk or interface defects. The extra incorporation of H can be thermally annealed later [62]. Our results give a lower limit of H_2 pressure. The critical temperatures, i.e., the maximum growth temperature by using the H surfactant effect for the layer by layer growth of $(000\bar{1})$-oriented GaN on the $-c$ plane of ZnO, are estimated and shown in Table II. For all of the sampling points, the differences of $\Delta\mu_H$ between GGA and HSE are reasonably small, within 110 meV, the difference in estimated critical temperatures from GGA and HSE are within 100 K. For A/A′, B/B′, and C/C′, the critical temperatures are about 1300 $\sim$ 1400 K. It should be noted that for D/D′, the critical temperature is around 1000 $\sim$ 1100 K, so the condition of D/D′ cannot be applied directly with the standard OMVPE temperature, $T = 1300$ K.

We note that the Ga-rich condition is mainly applied in most growth techniques to yield good crystal quality and flat surfaces; the growth condition near D/D′ is preferred from the crystal quality point of view. In such region near the Ga-rich condition, detrimental deep defects such as N_{Ga}, V_{Ga}, or V_{Ga}-H related complexes can be suppressed to a certain degree. The interplay of the H passivation between surfaces and point defects nearby is an interesting problem to be discovered, yet out of scope of this paper. Additionally, the growth temperature strongly influences the surface morphology and affects the optical properties of the GaN epitaxial films [100]. For other three points, especially A/A′ and B/B′, i.e., the growth window near N-rich and O-poor conditions, wider flexibility of controlling the growth temperature can be achieved. The relatively lower critical temperature at point D/D′ is also beneficial to the stability of pregrown ZnO buffer layers or substrates.

In the recent years, the topic of growing N-polar GaN with comparable high crystal quality to Ga-polar GaN has attracted much attention [101–103], due to the special advantages of N-polar thin films over Ga-polar ones [43,104–107]. Mg, In, and Si are used to assist to get rid of the disadvantages of the N-polar film growth on traditional sapphire and SiC substrates [102,108]. Our results predict that N-polar GaN of high crystal quality is very likely to be grown on ZnO O-polar substrates. This work may provide a new method to achieve this goal, and further investigations on the effect of growth conditions based on our results are necessary. Also, in addition to H, other group-I or valence-I elements can be attractive surfactant candidates that can be investigated in the future.

IV. CONCLUSION

In summary, the hydrogen surfactant effect was investigated and the wetting conditions of ZnO/GaN heterostructures are determined for the first time from first-principles using GGA and HSE functionals. We proposed a new strategy to accurately estimate the interface energy. A phase diagram of the sharp interface is obtained. Within this nearly N-rich and O-poor growth window, the absolute surface energies of the related reconstructed surfaces are obtained, as well as the absolute interface energies with possible configurations. It is confirmed from the wetting conditions that the growth of high-quality GaN thin films on ZnO substrates is difficult without surfactant. To turn over the wetting conditions, we proposed hydrogen as surfactant during the growth due to its advantages over other elements. When H-involved surface passivation is considered, with detailed analyses of atomistic thermodynamics, we predicted the proper growth conditions in which H surfactant can effectively alter the epitaxial growth mode, making it possible for GaN to achieve layer by layer growth mode on the $(000\bar{1})$ surface of ZnO. Our work may benefit the applications of GaN and related ZnO/GaN heterostructure devices, open up ZnO as a possible substrate or interlayer during GaN growth. This may reduce the usage of expensive substrates and gallium element in buffer layers. Such surfactant effect analysis shed light on further investigations of the surfactant-assisted heterostructure growth, especially for complex compounds.

ACKNOWLEDGMENTS

Part of the computing resources was provided by the High-Performance Cluster Computing Centre, Hong Kong Baptist University. This work was supported by the start-up funding, HKRGC funding with the Project code of 2130490, and direct grant with the Project code of 4053233, 4053134, and 3132748 at CUHK.

[1] S. Nakamura, T. Mukai, and M. Senoh, Appl. Phys. Lett. **64**, 1687 (1994).
[2] S. Nakamura, M. Senoh, N. Iwasa, and S.-i. Nagahama, Jpn. J. Appl. Phys., Part 2 **34**, L797 (1995).
[3] R. Vispute, V. Talyansky, S. Choopun, R. Sharma, T. Venkatesan, M. He, X. Tang, J. Halpern, M. Spencer, and Y. Li, Appl. Phys. Lett. **73**, 348 (1998).
[4] S. Nakamura, Science **281**, 956 (1998).
[5] D. C. Look, Mater. Sci. Eng. B **80**, 383 (2001).
[6] G. Stringfellow, J. Cryst. Growth **312**, 735 (2010).
[7] M. Nyk, R. Kudrawiec, J. Misiewicz, R. Paszkiewicz, R. Korbutowicz, J. Kozlowski, J. Serafinczuk, and W. Strek, J. Cryst. Growth **277**, 149 (2005).
[8] T. Paskova, D. A. Hanser, and K. R. Evans, Proc. IEEE **98**, 1324 (2010).
[9] J. H. Choi, A. Zoulkarneev, S. I. Kim, C. W. Baik, M. H. Yang, S. S. Park, H. Suh, U. J. Kim, H. B. Son, and J. S. Lee, Nat. Photonics **5**, 763 (2011).
[10] B. Nikoobakht, J. Bonevich, and A. Herzing, J. Phys. Chem. C **115**, 9961 (2011).
[11] X. Wang, X. Wang, J. Song, P. Li, J. H. Ryou, R. D. Dupuis, C. J. Summers, and Z. L. Wang, J. Am. Chem. Soc. **127**, 7920 (2005).
[12] Y. Xia, J. Brault, B. Damilano, S. Chenot, P. Vennéguès, M. Nemoz, M. Teisseire, M. Leroux, R. Obrecht, and I.-C. Robin, Appl. Phys. Express **6**, 042101 (2013).
[13] M. Leszczynski, H. Teisseyre, T. Suski, I. Grzegory, M. Bockowski, J. Jun, S. Porowski, K. Pakula, J. Baranowski, and C. Foxon, Appl. Phys. Lett. **69**, 73 (1996).

[14] Y.-I. Kim, K. Page, and R. Seshadri, Appl. Phys. Lett. **90**, 101904 (2007).

[15] T. Sekiguchi, S. Miyashita, K. Obara, T. Shishido, and N. Sakagami, J. Cryst. Growth **214-215**, 72 (2000).

[16] E. Ohshima, H. Ogino, I. Niikura, K. Maeda, M. Sato, M. Ito, and T. Fukuda, J. Cryst. Growth **260**, 166 (2004).

[17] K. Maeda, M. Sato, I. Niikura, and T. Fukuda, Semicond. Sci. Technol. **20**, S49 (2005).

[18] V. Avrutin, G. Cantwell, J. Zhang, J. Song, D. J. Silversmith, and H. Morkoç, Proc. IEEE **98**, 1339 (2010).

[19] R. Triboulet, Prog. Cryst. Growth Charact. Mater. **60**, 1 (2014).

[20] J. Liu, A. Kobayashi, J. Ohta, H. Fujioka, and M. Oshima, Appl. Phys. Lett. **103**, 172101 (2013).

[21] E. Hellman, D. Buchanan, D. Wiesmann, and I. Brener, MRS Internet J. Nitride Semicond. Res. **1**, e16 (1996).

[22] X. W. Sun, R. F. Xiao, and H. S. Kwok, J. Appl. Phys. **84**, 5776 (1998).

[23] F. Hamdani, M. Yeadon, D. J. Smith, H. Tang, W. Kim, A. Salvador, A. Botchkarev, J. Gibson, A. Polyakov, and M. Skowronski, J. Appl. Phys. **83**, 983 (1998).

[24] X. Gu, M. A. Reshchikov, A. Teke, D. Johnstone, H. Morkoc, B. Nemeth, and J. Nause, Appl. Phys. Lett. **84**, 2268 (2004).

[25] T. Suzuki, C. Harada, H. Goto, T. Minegishi, A. Setiawan, H. Ko, M.-W. Cho, and T. Yao, Current Applied Physics **4**, 643 (2004).

[26] A. Kobayashi, Y. Kawaguchi, J. Ohta, H. Fujioka, K. Fujiwara, and A. Ishii, Appl. Phys. Lett. **88**, 181907 (2006).

[27] N. Li, E.-H. Park, Y. Huang, S. Wang, A. Valencia, B. Nemeth, J. Nause, and I. Ferguson, Growth of GaN on ZnO for solid state lighting applications, in *Sixth International Conference on Solid State Lighting Proceedings of the SPIE, Vol. 6337* (SPIE, Bellingham, 2006), p. 63370Z.

[28] A. Kobayashi, Y. Shirakura, K. Miyamura, J. Ohta, and H. Fujioka, J. Cryst. Growth **305**, 70 (2007).

[29] A. Ougazzaden, D. Rogers, F. H. Teherani, T. Moudakir, S. Gautier, T. Aggerstam, S. O. Saad, J. Martin, Z. Djebbour, and O. Durand, J. Cryst. Growth **310**, 944 (2008).

[30] S.-K. Hong, T. Hanada, H.-J. Ko, Y. Chen, T. Yao, D. Imai, K. Araki, and M. Shinohara, Appl. Phys. Lett. **77**, 3571 (2000).

[31] S.-H. Hwang, T.-H. Chung, and B.-T. Lee, Mater. Sci. Eng. B **157**, 32 (2009).

[32] J. Von Pezold and P. Bristowe, J. Mater. Sci. **40**, 3051 (2005).

[33] C. Pan, C. Tu, C. Tun, C. Lee, and G. Chi, J. Cryst. Growth **305**, 133 (2007).

[34] X. Wang, H. Sun, and X. Pan, Appl. Phys. Lett. **97**, 151908 (2010).

[35] D. Adolph and T. Ive, Appl. Surf. Sci. **307**, 438 (2014).

[36] J. Zhang, Y. Zhang, K. Tse, B. Deng, H. Xu, and J. Zhu, J. Appl. Phys. **119**, 205302 (2016).

[37] M. Copel, M. C. Reuter, E. Kaxiras, and R. M. Tromp, Phys. Rev. Lett. **63**, 632 (1989).

[38] F. K. LeGoues, M. Copel, and R. Tromp, Phys. Rev. Lett. **63**, 1826 (1989).

[39] J. Y. Zhu, F. Liu, and G. Stringfellow, Phys. Rev. Lett. **101**, 196103 (2008).

[40] J. Zhu, F. Liu, and G. Stringfellow, J. Cryst. Growth **312**, 174 (2010).

[41] J. Zhu and S.-H. Wei, Front. Mater. Sci. **5**, 335 (2011).

[42] Y. Zhang, K. Tse, X. Xiao, and J. Zhu, Phys. Rev. Mater. **1**, 045403 (2017).

[43] Y. Zhang and J. Zhu, J. Cryst. Growth **438**, 43 (2016).

[44] D. C. Chapman, A. D. Howard, and G. B. Stringfellow, J. Cryst. Growth **287**, 647 (2006).

[45] A. D. Howard, D. C. Chapman, and G. B. Stringfellow, J. Appl. Phys. **100**, 044904 (2006).

[46] L. Zhang, Y. Yan, and S.-H. Wei, Phys. Rev. B **80**, 073305 (2009).

[47] E. Rudkevich, F. Liu, D. E. Savage, T. F. Kuech, L. McCaughan, and M. G. Lagally, Phys. Rev. Lett. **81**, 3467 (1998).

[48] J. Neugebauer and C. G. Van de Walle, Phys. Rev. Lett. **75**, 4452 (1995).

[49] J. Zhang, K. Tse, M. Wong, Y. Zhang, and J. Zhu, Frontiers of Physics **11**, 1 (2016).

[50] G. B. Stringfellow, *Organometallic Vapor-Phase Epitaxy: Theory and Practice* (Academic Press, New York, 1999).

[51] B. Meyer and D. Marx, Phys. Rev. B **67**, 035403 (2003).

[52] B. Meyer, Phys. Rev. B **69**, 045416 (2004).

[53] M. Valtiner, M. Todorova, G. Grundmeier, and J. Neugebauer, Phys. Rev. Lett. **103**, 065502 (2009).

[54] J. V. Lauritsen, S. Porsgaard, M. K. Rasmussen, M. C. Jensen, R. Bechstein, K. Meinander, B. S. Clausen, S. Helveg, R. Wahl, and G. Kresse, ACS nano **5**, 5987 (2011).

[55] R. Wahl, J. V. Lauritsen, F. Besenbacher, and G. Kresse, Phys. Rev. B **87**, 085313 (2013).

[56] R. Jacobs, B. Zheng, B. Puchala, P. M. Voyles, A. B. Yankovich, and D. Morgan, J. Phys. Chem. Lett. **7**, 4483 (2016).

[57] C. G. Van de Walle and J. Neugebauer, Phys. Rev. Lett. **88**, 066103 (2002).

[58] C. E. Dreyer, A. Janotti, and C. G. Van de Walle, Phys. Rev. B **89**, 081305 (2014).

[59] M. D. Pashley, Phys. Rev. B **40**, 10481 (1989).

[60] S. J. Pearton and A. J. Tavendale, Phys. Rev. B **26**, 7105 (1982).

[61] A. Hierro, S. Ringel, M. Hansen, J. Speck, U. Mishra, and S. DenBaars, Appl. Phys. Lett. **77**, 1499 (2000).

[62] S. Nakamura, N. Iwasa, M. Senoh, and T. Mukai, Jpn. J. Appl. Phys. **31**, 1258 (1992).

[63] J. E. Northrup, R. Di Felice, and J. Neugebauer, Phys. Rev. B **56**, R4325 (1997).

[64] K. Reuter and M. Scheffler, Phys. Rev. B **65**, 035406 (2001).

[65] K. Reuter and M. Scheffler, Phys. Rev. Lett. **90**, 046103 (2003).

[66] M. Valtiner, M. Todorova, and J. Neugebauer, Phys. Rev. B **82**, 165418 (2010).

[67] J. E. Northrup and J. Neugebauer, Appl. Phys. Lett. **85**, 3429 (2004).

[68] S.-J. Kahng, Y. H. Ha, J.-Y. Park, S. Kim, D. W. Moon, and Y. Kuk, Phys. Rev. Lett. **80**, 4931 (1998).

[69] J. Zhang, Y. Zhang, K. Tse, H. Xu, and J. Zhu, in *Chinese Physical Society Fall Meeting* (CPS, Changchun, 2015). The authors presented this method in Chinese Physical Society Fall Meeting in 2015. The talk was entitled Theoretical Investigation of Epitaxial Growth Mechanism for ZnO and GaN Heterostructures: Form a Sight of Surface and Interface Energies. While the manuscript was still under preparation, a work on interface energy calculation with the similar spirit was published recently, as shown in Ref. [70].

[70] T. Akiyama, H. Nakane, K. Nakamura, and T. Ito, Phys. Rev. B **94**, 115302 (2016).

[71] Y. Zhang, J. Zhang, K. Tse, L. Wong, C. Chan, B. Deng, and J. Zhu, Sci. Rep. **6**, 20055 (2016).

[72] D. Segev and C. G. Van de Walle, Surf. Sci. **601**, L15 (2007).

[73] H. Xu, L. Dong, X. Q. Shi, M. Van Hove, W. K. Ho, N. Lin, H. S. Wu, and S. Y. Tong, Phys. Rev. B **89**, 235403 (2014).

[74] K. Shiraishi, J. Phys. Soc. Jpn. **59**, 3455 (1990).

[75] C. Tang, M. J. Spencer, and A. S. Barnard, Phys. Chem. Chem. Phys. **16**, 22139 (2014).

[76] A. B. Yankovich, B. Puchala, F. Wang, J.-H. Seo, D. Morgan, X. Wang, Z. Ma, A. V. Kvit, and P. M. Voyles, Nano lett. **12**, 1311 (2012).

[77] R. R. Wixom, G. B. Stringfellow, and N. A. Modine, Phys. Rev. B **64**, 201322 (2001).

[78] R. R. Wixom, N. A. Modine, and G. Stringfellow, Phys. Rev. B **67**, 115309 (2003).

[79] P. Hohenberg and W. Kohn, Phys. Rev. **136**, B864 (1964).

[80] W. Kohn and L. J. Sham, Phys. Rev. **140**, A1133 (1965).

[81] G. Kresse and J. Furthmüller, Comput. Mater. Sci. **6**, 15 (1996).

[82] P. E. Blöchl, Phys. Rev. B **50**, 17953 (1994).

[83] G. Kresse and D. Joubert, Phys. Rev. B **59**, 1758 (1999).

[84] J. P. Perdew, K. Burke, and M. Ernzerhof, Phys. Rev. Lett. **77**, 3865 (1996).

[85] J. Heyd, G. E. Scuseria, and M. Ernzerhof, J. Chem. Phys. **118**, 8207 (2003).

[86] J. Heyd, G. E. Scuseria, and M. Ernzerhof, J. Chem. Phys. **124**, 219906 (2006).

[87] N. Jiang, J. L. Roehl, S. V. Khare, D. G. Georgiev, and A. H. Jayatissa, Thin Solid Films **564**, 331 (2014).

[88] S. Lany, Phys. Rev. B **78**, 245207 (2008).

[89] V. Stevanović, S. Lany, X. Zhang, and A. Zunger, Phys. Rev. B **85**, 115104 (2012).

[90] H. Peng, D. O. Scanlon, V. Stevanovic, J. Vidal, G. W. Watson, and S. Lany, Phys. Rev. B **88**, 115201 (2013).

[91] See Supplemental Material at http://link.aps.org/supplemental/10.1103/PhysRevMaterials.2.013403 for summary of the FERE method calculation details, the effects of absolute surface energy changes after applying the FERE method, and the discussions of H surfactant effect on c plane of GaN and ZnO.

[92] O. Kubaschewski, C. B. Alcock, and P. J. Spencer, *Materials Thermochemistry* (Pergamon Press, New York, 1993), pp. 279–321.

[93] M. R. Ranade, F. Tessier, A. Navrotsky, V. J. Leppert, S. H. Risbud, F. J. DiSalvo, and C. M. Balkas, J. Phys. Chem. B **104**, 4060 (2000).

[94] M. W. Chase, C. A. Davies, J. R. Downey, D. J. Frurip, R. A. Mcdonald, and A. N. Syverud, *NIST-JANAF Thermodynamic Tables*, Fourth Edition (NIST, Gaithersburg, MD, 1998) [J. Phys. Chem. Ref. Data Monograph **9**, 1343 (1998)].

[95] Y.-J. Wu, C.-H. Liao, C.-Y. Hsieh, P.-M. Lee, Y.-S. Wei, Y.-S. Liu, C.-H. Chen, and C.-Y. Liu, J. Phys. Chem. C **119**, 5122 (2015).

[96] J. Lei, D.-P. Zhu, M.-C. Xu, and S.-J. Hu, Phys. Lett. A **379**, 2384 (2015).

[97] C. Kittel and H. Kroemer, *Thermal Physics*, Vol. 9690 (Wiley, New York 1973), pp. 169–171.

[98] D. V. Schroeder, *Thermal physics*, (AddisonWesley Pub Co., San Francisco, 2000), pp. 251–255.

[99] I. Barin, in *Thermochemical Data of Pure Substances* (Wiley-VCH, Verlag GmbH, 2008), p. 781.

[100] S. Kushvaha, P. Pal, A. Shukla, A. G. Joshi, G. Gupta, M. Kumar, S. Singh, B. K. Gupta, and D. Haranath, AIP Adv. **4**, 027114 (2014).

[101] Q. Sun, Y. S. Cho, B. H. Kong, H. K. Cho, T. S. Ko, C. D. Yerino, I.-H. Lee, and J. Han, J. Cryst. Growth **311**, 2948 (2009).

[102] D. Won, X. Weng, and J. M. Redwing, Appl. Phys. Lett. **100**, 021913 (2012).

[103] Q. Sun, Y. Cho, I.-H. Lee, J. Han, B. Kong, and H. Cho, Appl. Phys. Lett. **93**, 131912 (2008).

[104] S. Rajan, A. Chini, M. H. Wong, J. S. Speck, and U. K. Mishra, J. Appl. Phys. **102**, 044501 (2007).

[105] M. Stutzmann, O. Ambacher, M. Eickhoff, U. Karrer, A. Lima Pimenta, R. Neuberger, J. Schalwig, R. Dimitrov, P. Schuck, and R. Grober, Phys. Status Solidi B **228**, 505 (2001).

[106] N. A. Fichtenbaum, C. Schaake, T. E. Mates, C. Cobb, S. Keller, S. P. DenBaars, and U. K. Mishra, Appl. Phys. Lett. **91**, 172105 (2007).

[107] J. Simon, V. Protasenko, C. Lian, H. Xing, and D. Jena, Science **327**, 60 (2010).

[108] P. Tavernier, T. Margalith, J. Williams, D. Green, S. Keller, S. DenBaars, U. Mishra, S. Nakamura, and D. Clarke, J. Cryst. Growth **264**, 150 (2004).